JCTC Journal of Chemical Theory and Computation

Article

pubs.acs.org/JCTC

Three-Dimensional RISM Integral Equation Theory for Polarizable Solute Models

Franziska Hoffgaard, Jochen Heil, and Stefan M. Kast*

Physikalische Chemie III, TU Dortmund, Otto-Hahn-Str. 6, 44227 Dortmund, Germany

ABSTRACT: Modeling solute polarizability is a key ingredient for improving the description of solvation phenomena. In recent years, polarizable molecular mechanics force fields have emerged that circumvent the limitations of classical fixed charge force fields by the ability to adapt their electrostatic potential distribution to a polarizing environment. Solvation phenomena are characterized by the solute's excess chemical potential, which can be computed by expensive fully atomistic free energy simulations. The alternative is to employ an implicit solvent model, which poses a challenge to the formulation of the solute−solvent interaction term within a polarizable framework. Here, we adapt the three-dimensional reference interaction site model (3D RISM) integral equation theory as a solvent model, which analytically yields the chemical potential, to the polarizable AMOEBA force field using an embedding cluster (EC-RISM) strategy. The methodology is analogous to our earlier approach to the coupling of a quantum-chemical solute description with a classical 3D RISM solvent. We describe the conceptual physical and algorithmic basis as well as the performance for several benchmark cases as a proof of principle. The results consistently show reasonable agreement between AMOEBA and quantum-chemical free energies in solution in general and allow for separate assessment of energetic and solvation-related contributions. We find that, depending on the parametrization, AMOEBA reproduces the chemical potential in better agreement with reference quantum-chemical calculations than the intramolecular energies, which suggests possible routes toward systematic improvement of polarizable force fields.

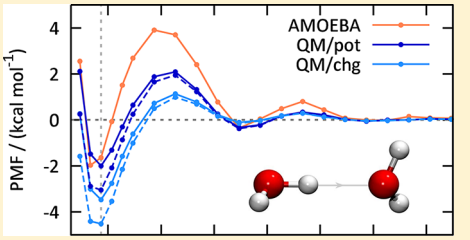

INTRODUCTION

In traditional classical mechanical force fields, the electrostatic molecular interactions are described by fixed atom charges that are usually placed on atom centers. Although environmental polarization is usually effectively included during the charge parametrization process, such a description is inherently limited since it lacks the ability to dynamically adapt to local details of a fluctuating environment exhibited by a solvent or the intramolecular neighborhood. Adding explicit molecular polarizability to the molecular model may account for the proper response of a molecule's electrostatic potential distribution to environmental variations. Most prominent among the available polarization models are the Drude oscillator, the fluctuating charge, and the inducible point dipole model.[1,2] For Drude oscillators,[3−6] polarization is modeled by attaching a massless charged particle via a harmonic spring to each polarizable site. In contrast, fluctuating charge models[7−10] incorporate polarization in the standard energy functions by allowing local partial charge values to fluctuate. The induced point dipole model[11−14] utilizes both partial charges and inducible dipoles and is incorporated in a number of polarizable force fields. Among others, the "atomic multipole optimized energetics for biomolecular applications" (AMOEBA)[15−19] model makes use of this approach. Herein, atom-centered multipole moments up to quadrupoles contribute to the permanent electrostatic interaction potential. Additionally, inducible dipoles respond to changes due to an external field.

In recent years, numerous works have illustrated the relevance of polarizable force fields for the prediction of physicochemical properties on different length scales, including for instance studies on solvation free energies of ions[20−24] and on conformational minima of small model peptides and organic molecules.[25−27] AMOEBA-derived solvation free energies of a variety of small organic molecules in the context of the SAMPL-2 prediction challenge showed good agreement with experimental values.[15] Most of those studies were performed by means of molecular dynamics (MD) simulations and thermodynamic integration with an explicit, polarizable solvent model. Until now, only a few studies[28−31] adopted polarizable force fields in combination with dielectric continuum solvation models in the context of Poisson−Boltzmann theory.

Combinations with granular implicit solvation models, such as the 3D RISM (reference interaction site model),[32,33] have not been described yet. Dielectric continuum models lack granular solvent features necessary to adequately delineate local and directional solvation features such as H-bonding that result from anisotropic solvent distributions. In this respect, 3D RISM theory represents a liquid state theory that yields the spatial distribution of solvent sites on a 3D grid around the solute molecule. The solvent employed in this context is typically an established fixed charge molecular model as used in common MD simulations. If applied to a solute model with given electrostatic solute−solvent interaction, 3D RISM theory yields the excess chemical potential (equivalent to the solvation free energy if intramolecular relaxation upon solvation is ignored)

Received: August 6, 2013

   dx.doi.org/10.1021/ct400699q | J. Chem. Theory Comput. XXXX, XXX, XXX−XXX

Table 1. Different Setups for the Parametrization of Small Organic Molecules[a]

	initial multipoles	torsion scan	electrostatic potential
AMOEBA/P1(a)	MP2/6-311G*	M06L/6-31G**	MP2/6-311++G(2d,2p)
AMOEBA/P1(b)	MP2/6-311G*	MP2/6-311++G(2d,2p)	MP2/6-311++G(2d,2p)
AMOEBA/P2(a)	MP2/6-311++G(2d,2p)	M06L/6-31G**	MP2/6-311++G(2d,2p)
AMOEBA/P2(b)	MP2/6-311++G(2d,2p)	MP2/6-311++G(2d,2p)	MP2/6-311++G(2d,2p)
AMOEBA/P3(a)	MP2/aug-cc-pVTZ	M06L/6-31G**	MP2/aug-cc-pVTZ
AMOEBA/P3(b)	MP2/aug-cc-pVTZ	MP2/6-311++G(2d,2p)	MP2/aug-cc-pVTZ

[a]The basis sets employed within the POLTYPE parametrization schemes are given both for the single point evaluation, which is used to derive initial multipole components for each atomic site, and for the electrostatic potential that is used for refining the atomic multipoles. The parametrization schemes employed are referred to as AMOEBA/P1−P3 with identifiers (a) and (b) denoting the default torsion scan level of theory and a higher level corresponding to EC-RISM/QM calculations, respectively.

analytically as a functional of solute−solvent correlation functions. Solute polarizability can be accounted for iteratively by solving the integral equations for the solvent distribution in mutual consistency with the solute's electrostatic potential distribution. Such an approach has been described by us[34] earlier for a quantum-mechanical (QM) description of the solute such that the solute's electronic and the solvent structure are treated self-consistently in this case. Electronic and solvent structure are coupled by mapping the electrostatic potential exhibited by the solvent distribution, which is computed from 3D RISM theory, onto a set of discrete background charges that polarize the electronic solute Hamiltonian, giving rise to the acronym "EC-(embedded cluster-) RISM" theory. In turn, the solute's charge distribution responds to the solvent polarization, which modulates the solvent distribution, thus defining the iteration cycles that are repeated until both solute electronic and solvent structure are consistent to within a prescribed accuracy. The QM formulation of EC-RISM has been shown to be capable of predicting tautomer ratios and pK_a shifts[34,35] in water with high accuracy.

Here, we basically transfer the cluster embedding strategy to a classical polarizable solute model. The underlying idea of approximating the potential distribution arising from the electronic structure of a solute by a polarizable force field is based on the formal equivalence between the relaxation of a wave function and of local atomic polarizability terms in the presence of an anisotropic external, solvent-generated electric field. In addition, the enhanced flexibility of local atomic multipoles that govern the accurate representation of the intramolecular potential distribution is a further benefit over common fixed charge force fields. In this study, we demonstrate the performance of EC-RISM in conjunction with the polarizable AMOEBA force field. To this end, we extended the EC-RISM framework by adding modified TINKER[36] routines to incorporate AMOEBA in analogy to a quantum chemistry software. The performance is assessed by application to various benchmark systems in water. The standard reaction free energy of the *gauche*−*trans* equilibrium of 1,2-dichloroethane is computed and compared with experimental and previously calculated results.[34] Furthermore, we determine the performance of AMOEBA in comparison with fixed charge force fields to predict relative conformational energies of the alanine dipeptide, and we compute the potential of mean force for a water dimer. All EC-RISM/AMOEBA data are benchmarked against reference EC-RISM/QM calculations. We also dissect solvation and energetic terms in order to suggest routes for further improvements.

METHODS

AMOEBA. The polarizable force field AMOEBA was developed by Ponder and co-workers[15−18] and adopts the following functional form to describe interactions among atoms:

$$E = E_{\text{bond}} + E_{\text{angle}} + E_{b\theta} + E_{\text{oop}} + E_{\text{torsion}} + E_{\text{vdw}} + E_{\text{ele}}^{\text{perm}} + E_{\text{ele}}^{\text{ind}} \quad (1)$$

where the first five terms describe covalent interactions (i.e. bond stretching, angle bending, bond-angle cross term, out-of-plane-bending, and torsional rotation). The nonbonded van der Waals interactions of two atoms are described by a buffered 14−7 potential with the respective mixing rules for heterogeneous atom pairs. Permanent and induced electrostatic contributions, $E_{\text{ele}}^{\text{perm}}$ and $E_{\text{ele}}^{\text{ind}}$, are described by interacting multipoles up to quadrupole moments placed on atomic sites. Dipoles are induced via a scheme first described by Applequist[37] leading to a self-consistent induction of all polarizable sites. A well-known artifact of point polarizability models is the so-called "polarization catastrophe" which occurs for interacting multipole sites at short-range yielding infinite interaction energies. Therefore, Thole proposed a damping approach, where the atomic multipole moments of one of the interacting sites are replaced by a smeared charge distribution.[38] For AMOEBA, the functional form of the investigated damping functions as well as corresponding atomic polarizabilities are adopted,[38,39] although the factor that effectively controls the damping strength has been altered for AMOEBA after fitting interaction energies for water clusters.[16,18] For further details, see Ponder et al.[15]

Parametrization of Organic Molecules. Since parameters for only a limited number of organic compounds are already available within the AMOEBA force field, electrostatic and valence parameters need to be derived for yet unknown organic species. Therefore, Ren et al.[16] suggested a detailed parametrization protocol that is implemented in POLTYPE[40] based on the QM software Gaussian09[41] and that proceeds as follows: (i) Starting from an arbitrary structure, a QM geometry optimization is performed, or the respective Gaussian09 output containing the optimized structure is required. (ii) Initial multipole components are obtained from a QM single point calculation via Gaussian distributed multipole analysis (GDMA).[42−44] After averaging multipoles for equivalent atoms, the nonzero dipole, and quadrupole components are refined by least-squares fitting to the QM electrostatic potential computed on a grid outside the van der Waals surface of the molecule, which is defined by Bondi radii.[45] (iii) Valence parameters are then derived by a SMARTS string lookup in the

dx.doi.org/10.1021/ct400699q | J. Chem. Theory Comput. XXXX, XXX, XXX−XXX

AMOEBA-2009 force field and a subsequent torsional scan of rotational bonds to best fit conformational energies computed by QM at the M06L/6-31G** (default) or a user-specified level of theory.

Geometry optimizations prior to parametrization were performed by MP2/6-311++G(2d,2p) calculations *in vacuo*. Following earlier studies on the performance of different basis sets for parametrizing small organic molecules,[27,46] we employed different levels of theory with the MP2 electron density for the single point evaluations to extract initial multipoles, for the torsion scan to adapt the conformational energies and for the electrostatic potential needed for the refinement of the multipole parameters (see Table 1). Torsion scans were computed using both the default settings and a higher level that corresponds to the EC-RISM/QM reference calculations of the intramolecular energies. Note that we used the original DMA method throughout despite its known deficiencies for basis sets containing diffuse functions[27] just in order to test the performance particularly for the chemical potential.

3D RISM. The solvent site density $\rho_\gamma g_\gamma(\mathbf{r})$ at a spatial point $\mathbf{r}$ can approximately be described by the 3D RISM equations which couple the total and direct correlation functions, $h_\gamma(\mathbf{r})$ and $c_\gamma(\mathbf{r})$, between a solute molecule and solvent sites via

$$\rho_\gamma h_\gamma(\mathbf{r}) = \sum_{\gamma'} c_{\gamma'} * \chi_{\gamma\gamma'}(\mathbf{r}) \tag{2}$$

$\chi_{\gamma\gamma'}(\mathbf{r})$ is the solvent site susceptibility from 1D RISM pure solvent calculations, and the star means convolution. The pair distribution function g_γ is connected to the total correlation function h_γ by the relation $g_\gamma = h_\gamma + 1$. To solve the integral equations, a so-called closure relation is needed. Here, we use the partial series expansion of order n (PSE-n)[47] of the hypernetted chain (HNC) closure[48,49]

$$h_\gamma(\mathbf{r}) = \begin{cases} \exp(d_\gamma(\mathbf{r})) - 1 & \Leftrightarrow \; d_\gamma(\mathbf{r}) \le 0 \\ \sum_{i=0}^{n} (d_\gamma(\mathbf{r}))^i / i! - 1 & \Leftrightarrow \; d_\gamma(\mathbf{r}) > 0 \end{cases}$$

$$d_\gamma(\mathbf{r}) = -\beta u_\gamma(\mathbf{r}) + h_\gamma(\mathbf{r}) - c_\gamma(\mathbf{r}) \tag{3}$$

where $\beta = (k_B T)^{-1}$ with the Boltzmann constant k_B. We[47] and others[50] independently have shown that PSE beyond first oder, which was employed throughout in this work, yields thermodynamic quantities in close agreement with HNC results while numerical instability frequently encountered with HNC is effectively avoided. Case and co-workers,[50] moreover, compared integral equation and MD data for ion activities and found reasonably good agreement.

The interaction potential $u_\gamma(\mathbf{r})$ between solvent site γ and the solute can be split into a short-ranged potential $u_\gamma^S(\mathbf{r})$ and a corresponding long-range part $u_\gamma^L(\mathbf{r})$, yielding $u_\gamma(\mathbf{r}) = u_\gamma^S(\mathbf{r}) + u_\gamma^L(\mathbf{r})$. The electrostatic part of the interaction potential is determined self-consistently during EC-RISM iterations. It is based on the electrostatic solute potential ϕ specified on a 3D grid, which, for practical reasons, is subdivided into two components as

$$\phi(\mathbf{r}) = \phi^{pc}(\mathbf{r}) + \Delta\phi(\mathbf{r}) \tag{4}$$

The first component of this renormalization ansatz is the electrostatic potential originating from partial site charges that are fitted to represent approximately the exact potential, $\phi^{pc}(\mathbf{r})$, such that the second component is short-ranged. The electrostatic Coulomb interaction with a solvent charge q_γ from the point charge potential, $u_\gamma^C(\mathbf{r}) = q_\gamma \phi^{pc}(\mathbf{r})$ is, as usual, evaluated by Ewald summation; that is, it is further split into a short-range part $u_\gamma^{C,S}(\mathbf{r})$ and a corresponding long-range part $u_\gamma^{C,L}(\mathbf{r})$, that is evaluated in reciprocal space. Hence, the short-range interaction potential $u_\gamma^S(\mathbf{r})$ is defined by

$$u_\gamma^S(\mathbf{r}) = u_\gamma^{LJ}(\mathbf{r}) + q_\gamma \Delta\phi(\mathbf{r}) + u_\gamma^{C,S}(\mathbf{r}) \tag{5}$$

A similar subdivision is applied for EC-RISM/QM calculations with the exact QM electrostatic potential.

Two issues are important to note here. First, since we employ common molecular mechanics fixed charge water solvent models as in our earlier EC-RISM/QM calculations, the repulsion−dispersion interactions in 3D RISM are described by a 12−6 Lennard-Jones potential. This facilitates direct comparison with EC-RISM/QM results although an inconsistency with the original AMOEBA parametrization arises, which could be crucial since polarization is already contained effectively in the 12−6 terms as a result of the parametrization process for fixed charge force fields. Second, since the small difference between exact and point charge potential is aperiodic in contrast to all other terms (by definition in reciprocal space or by employing the minimum image convention for the repulsion-dispersion expression) the grid size has to be large enough such that $\Delta\phi$ has sufficiently decayed. Furthermore (although in the cases studied below this was not problematic), one has to make sure by refining the point charge component that negative values for $q_\gamma\Delta\phi$ do not cause overflow errors in the closure exponential.

Finally, from converged 3D RISM correlation functions the excess chemical potential μ^{ex} can be computed for PSE-n closures from

$$\mu_{PSE-n}^{ex} = \beta^{-1}\rho_\gamma \int d\mathbf{r}\Big[\frac{1}{2}h_\gamma^2(\mathbf{r}) - c_\gamma(\mathbf{r}) - \frac{1}{2}h_\gamma(\mathbf{r})c_\gamma(\mathbf{r}) - \Theta(h_\gamma(\mathbf{r}))(d_\gamma(\mathbf{r}))^{n+1}/(n+1)!\Big] \tag{6}$$

where Θ is the Heaviside step function.[47]

EC-RISM. The EC-RISM cycle in conjunction with AMOEBA is schematically sketched in analogy to the original QM coupling with 3D RISM calculation, as shown in Figure 1.[34] QM calculations within EC-RISM are replaced by the modified TINKER 6.0.12 routines *potential* and *analyze*. In each EC-RISM cycle, the potential energy E is computed with "frozen multipoles" using TINKER as defined by eq 1; in the initial vacuum step, no solvent-induced dipole effects are present. In this context, the term "frozen multipoles" refers to the permanent multipoles and the solvent-induced atomic dipoles $\{M\}_{solv}$ in the absence of the polarizing solvent background. The atom-centered charges needed for computing $\phi^{pc}(\mathbf{r})$ are derived by a least-squares fit to the "frozen multipoles" electrostatic potential on a subgrid outside the van der Waals surface of the solute molecule. The solvent response caused by altered electrostatic interactions, see eq 5, leads to a modified solvent site density distribution, which in turn responds upon the induction of the dipoles. Convergence is achieved if the sum of the potential energy E and the excess chemical potential μ^{ex} falls below a given threshold.

After convergence of the EC-RISM cycles the Gibbs energy ΔG for a reaction $A_{solv} \rightarrow B_{solv}$ is expressed as

dx.doi.org/10.1021/ct400699q | J. Chem. Theory Comput. XXXX, XXX, XXX−XXX

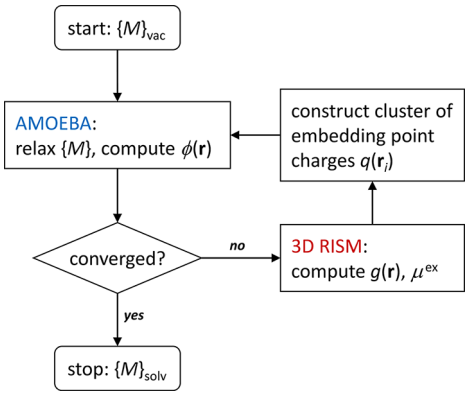

Figure 1. Flowchart for EC-RISM/AMOEBA calculations. Starting from a solute molecule *in vacuo*, the atomic multipoles are relaxed by responding to an external field originating from a set of background charges $q^{bg}(\mathbf{r}_i)$ on grid points $\mathbf{r}_i$ computed by approximately integrating the solvent site charge density over the grid point volume ΔV via $q^{bg}(\mathbf{r}_i) = \Delta V \sum_\gamma q_\gamma \rho_\gamma g_\gamma(\mathbf{r}_i)$. From the relaxed multipoles $\{M\}_{solv}$ the updated electrostatic potential ϕ along with corresponding partial charges is computed. This in turn affects the solvent's response from a new 3D RISM calculation leading to refined distribution functions, and, thus, to a new set of background charges that act upon the atomic multipoles.

$$\Delta G \approx \Delta E_{sol} + \Delta\mu^{ex} \quad (7)$$

where we ignore pressure−volume work and intramolecular entropic contributions. Here, $\Delta E_{sol} = E_{sol}(B) - E_{sol}(A)$ represents the difference of the intramolecular energies of A and B in solution, that is, the "frozen multipoles" energy excluding background charge interactions, and $\Delta\mu^{ex}$ is the respective difference in the excess chemical potentials, which is determined by 3D RISM correlation functions. If the thermodynamic solvent state corresponds to a pressure of 1 bar, the Gibbs reaction energy ΔG is equivalent to the standard reaction free energy ΔG° at the specified temperature which was set to 298.15 K throughout this work. Note that EC-RISM/AMOEBA calculations always employ the exact multipole-derived electrostatic interactions since the parametrization accounts for atomic monopoles and multipoles simultaneously while the polarizability is captured by inducible dipoles only. In contrast, EC-RISM/QM within the point charge approximation accounts for the polarizability during each iteration cycle by fitting atomic site charges for each solvent-induced potential distribution separately.

Computational Details of Benchmark Systems. We evaluated the performance of the EC-RISM/AMOEBA approach by treating three benchmark cases in water solution. The water model employed here (modified SPC/E[51]) and the corresponding pure solvent susceptibility as well as the 3D RISM procedural parameters were identical with those used in earlier EC-RISM/QM calculations for tautomer predictions.[35] All EC-RISM/QM calculations including ChelpG partial charge derivations were performed with Gaussian03;[52] the EC-RISM convergence tolerance was set to 0.001 kcal mol^{-1}.

To determine the standard reaction free energy of the *gauche*−*trans* equilibrium of 1,2-dichloroethane, *t*-$C_2H_4Cl_2$(sol) → *g*-$C_2H_4Cl_2$(sol), both molecules were parametrized individually using POLTYPE as described[40] before submitting them to EC-RISM/AMOEBA and EC-RISM/QM calculations. The latter were performed both with partial charges (as has been done in earlier work[34]) and with the exact quantum-chemical electrostatic potential at the MP2/6-311++G(2d,2p) level and using the MP2 electron density, employing a similar renormalization strategy as specified in eq 4. In each case, the box size was chosen with a minimum distance of the edges to any solute atom of 25 Å for the iteration and 30 Å for the final energy calculations with a grid spacing of 0.3 Å. PSE-3[47] was employed as closure. Lennard-Jones parameters for the solute description within 3D RISM were taken from the AMBER GAFF (June 2003) force field.[53]

In order to assess the importance of a polarizable solvent environment in comparison with our nonpolarizable solvent model for intramolecular solute energies, we additionally performed MD simulations of the two rigid dichloroethane conformations (AMOEBA/P2(a) parametrization) with both the original flexible and polarizable AMOEBA water model and with a frozen nonpolarizable variant. To this end, simulations in the canonical ensemble (30 Å × 30 Å × 30 Å simulation box corresponding to a water density of ca. 1 g cm^{-3}) at 298.15 K (Andersen thermostat) with a time step of 2 fs comprised one solute and 898 (*gauche*) and 900 (*trans*) water molecules, subject to Ewald summation (particle mesh on a 36 × 36 × 36 reciprocal space grid for monopole interactions, damping coefficient of 0.544 Å^{-1}) and a 9 Å real-space cutoff. The initial pure water simulation box (903 molecules) was minimized (L-BFGS) down to a root-mean-square gradient of 0.5 kcal mol^{-1} Å^{-1} during which electrostatic interactions were turned off. After placing the solute species by removing overlapping water, another minimization down to a gradient of 0.1 kcal mol^{-1} Å^{-1} was performed for both polarizable and nonpolarizable solvent variants. Simulations of the rigid body dynamics (also for polarizable AMOEBA water) were performed over 1 ns, while configurations were extracted every 0.1 ps skipping the first 20 ps of equilibration time. Average intrasolute energies were computed subject to a blocking analysis for the determination of the standard error.

For the second benchmark, three arbitrary conformations of the alanine dipeptide were generated in zwitterionic form. Subsequently, AMBER ff99SB[54,55] parameters were assigned and the three structures were subjected to a short energy minimization within AMBER[56] in a Generalized Born solvent[57] using default settings for 500 steps. For each structure, we performed three types of computations: 3D RISM using original Amber ff99SB nonbonded parameters, EC-RISM/QM using the exact electrostatic potential at the MP2/6-311++G(2d,2p) level of theory with the Hartree−Fock electron density, and EC-RISM with AMOEBA-BIO-2009 parameters. The AMBER-generated Lennard-Jones parameters were used in all calculations to describe solute−solvent interactions in 3D RISM. The box size for each case was fixed at 100 × 100 × 100 points with a spacing of 0.3 Å; PSE-2 was employed as closure.

In the last benchmark, we computed the potential of mean force (PMF) for a water dimer starting with a dimer geometry optimized using Gaussian03[52] at the MP2/6-311++G(2d,2p) level using the polarizable continuum model.[58] As reaction coordinate the axis between the O atom of one monomer and one H atom of the other monomer was defined (see below) with a minimum energy distance of 1.868 Å. Along this axis one of the molecules was moved in steps of 0.2 Å within the interval [−0.4 Å, 0.6 Å] and 0.4 Å within [1.0 Å, 8.2 Å]. For each point on the reaction coordinate EC-RISM calculations (AMOEBA and QM) were performed, the latter at the MP2/6-311++G(2d,2p) level with MP2 electron density by using both the exact potential and partial charges only. QM dimer energies are

dx.doi.org/10.1021/ct400699q | J. Chem. Theory Comput. XXXX, XXX, XXX−XXX

Table 2. Results for the *gauche*−*trans* Equilibrium of 1,2-Dichloroethane[a]

	ΔE_{vac}	$\Delta\mu^{ex}_{vac}$	ΔG°_{vac}	p_{vac} (g)	ΔE_{sol}	$\Delta\mu^{ex}_{sol}$	ΔG°_{sol}	p_{sol} (g)
QM/pot	1.45	−0.64	0.81	2.71	2.05	−1.55	0.51	3.49
QM/chg	1.45	−0.96	0.49	2.71	2.03	−1.97	0.05	3.64
AMOEBA/P1(a)	0.59	−0.73	−0.14	2.70	0.72	−1.73	−1.01	3.63
AMOEBA/P1(b)	1.97	−0.73	1.24	2.70	2.10	−1.73	0.37	3.63
AMOEBA/P2(a)	−1.51	−0.75	−2.26	2.71	−1.46	−1.71	−3.17	3.62
AMOEBA/P2(b)	0.27	−0.75	−0.48	2.71	0.32	−1.71	−1.39	3.62
AMOEBA/P3(a)	−1.48	−0.65	−2.12	2.70	−1.41	−1.61	−3.01	3.62
AMOEBA/P3(b)	0.11	−0.65	−0.54	2.70	0.18	−1.61	−1.43	3.62

[a]Data are shown for EC-RISM/QM calculations at MP2/6-311++G(2d,2p) with MP2 density for the exact potential (pot) as well as for derivation of partial charges (chg). For EC-RISM in combination with AMOEBA, we used different parametrization schemes P1(a,b)−P3(a,b) as explained in Table 1. All energies are listed in kcal mol^{-1}, the dipole moments of *gauche*-1,2-dichloroethane in vacuum $p_{vac}(g)$ and in solution $p_{sol}(g)$ are given in Debye. Experimental consensus value: −0.05 ± 0.05 kcal/mol.[34,59]

reported with and without accounting for the basis set superposition error (BSSE). The box size was fixed for all computations at 120 × 120 × 120 with a grid spacing of 0.3 Å; PSE-2 was used as closure. Analogous EC-RISM calculations were performed for each of the water monomers in order to define the reference energies. The Lennard-Jones parameters were identical with the surrounding modified SPC/E species.

RESULTS

***gauche*−*trans* Equilibrium of 1,2-Dichloroethane.** The EC-RISM results for both QM and AMOEBA coupling with different parametrization schemes P1(a,b)−P3(a,b) are summarized in Table 2. We observe only minor differences between the QM approaches. Employing partial charges ("QM/chg") reproduces essentially the data reported by Kloss et al.[34] (although in the original reference the hypernetted chain closure was applied to which PSE-3 represents a good approximation[47,50]). These data are close to experimental values while the results obtained with the exact potential ("QM/pot") are slightly worse but still within chemical accuracy compared to experimental data (the reason for this might be related to the spherically symmetric Lennard-Jones potential, which is parametrized in conjunction with atom-centered point charges, but in general, we do not observe a clear trend favoring one over the other electrostatics model). The polarizable force field approach with its different parametrizations is clearly able to capture the influence of the solvent, as illustrated by the change of the total dipole moment of the *gauche* conformation going from vacuum to solution. The increase is quantitatively similar to that observed with EC-RISM/QM.

The difference of Gibbs energies agrees well for parametrization P1(b) only but in other cases shows large deviations, even larger so for the solvated molecules. To clarify the source of this discrepancy, we specify the contributions to the Gibbs energy difference ΔG°, see eq 7, for vacuum and converged EC-RISM data. Obviously, the excess chemical potential differences $\Delta\mu^{ex}$ computed with various AMOEBA parameters resemble the QM results with almost negligible differences between the schemes employed. This finding is further illustrated by comparing the pair distribution function that is closely linked to μ^{ex} of QM and AMOEBA results, as shown in Figure 2. Here, we see for both the *trans* and the *gauche* conformations only minor differences between solvent density distributions obtained with EC-RISM/QM and the EC-RISM/AMOEBA. Thus, the reason for Gibbs energy deviations

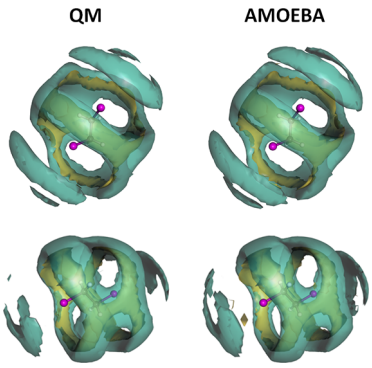

Figure 2. Pair distribution functions of 1,2-dichloroethane. For both the *gauche* (upper panels) and the *trans* conformation (lower panels) of 1,2-dichloroethane the three-dimensional pair distribution functions for both solvent sites O (yellow, isovalue 2.75 (*gauche*), 2.65 (*trans*)) and H (cyan, isovalue 1.3) are illustrated for converged EC-RISM calculations both with QM calculations using the exact potential and with AMOEBA/P2(a).

is rooted in the intramolecular solute energies ΔE_{sol}, which becomes obvious from Table 2.

For parametrizations P2 and P3, we find strong discrepancies compared to QM results, both for the vacuum and the solvated structures. Only P1 is able to capture the transition from *trans* to the *gauche* conformation in terms of the intramolecular solute energy, better so for variant (b) where the torsion energy effectively corrects the difference between initial force field and QM energies. This is, of course, not unexpected since we essentially measure the energetic accuracy of the default torsion scan in comparison with a higher level employed also in EC-RISM/QM. The deviation between P1 and P2/P3 is also reasonable since we used the original DMA method throughout for parametrizing AMOEBA terms, which is known not to deal well with diffuse functions in the basis set, in contrast to the more recent DMA2 procedure.[46] Interestingly, despite its deficiencies parametrizations P2 and P3 nevertheless reproduce the chemical potential quite well. For all AMOEBA setups the change in relative solute energies upon solvation, ΔE_{sol}-ΔE_{vac}, is only partially recovered, as seen by comparing values of about 0.5 kcal mol^{-1} obtained with QM and of about 0.05−0.15 kcal mol^{-1} with AMOEBA. One might attribute this discrepancy to known problems of AMOEBA with heavier halogen atoms.[15] One could alternatively come to the conclusion that the induced dipole interaction energy, which is the only term that changes upon transition from vacuum to solution with fixed geometry is not fully able to capture the changes in the

dx.doi.org/10.1021/ct400699q | J. Chem. Theory Comput. XXXX, XXX, XXX−XXX

electronic structure of the solute. Hence, an incorporation of polarizability effects into valence terms is presumably necessary to adjust the intramolecular solute energies, which has already been mentioned by Ren et al.[16] The alternative, varying polarizability parameters in order to improve intramolecular energies, would worsen the already very good quality of the chemical potential.

The MD simulations in both a polarizable and a nonpolarizable solvent confirm this interpretation. The average solute energies yield $\langle \Delta E_{pol} \rangle = (-1.408 \pm 0.014)$ kcal mol^{-1} and $\langle \Delta E_{nonpol} \rangle = (-1.368 \pm 0.009)$ kcal mol^{-1}, that is, only a small impact of explicit solvent polarizability, although the flexibility of AMOEBA water, which has been neglected here, could play a bigger role. Blocking analysis suggests a correlation time of about 0.8 ps (polarizable) and 0.4 ps (unpolarizable). These results agree with the conclusions of Shi et al.[46] who computed hydration free energies with both the AMOEBA water and a nonpolarizable water model based on AMOEBA. They showed that on average the deviation from experimental values was smaller for polarizable AMOEBA water, but the difference range between results for both water models was within 0.1 to 3 kcal mol^{-1}. Therefore, we may conclude that although repolarization effects are present if a polarizable solvent model is used, the approximation of a nonpolarizable solvent within EC-RISM should nevertheless lead to meaningful results.

Relative Conformational Energies of Alanine Dipeptide Structures. The three geometries are depicted in Figure 3

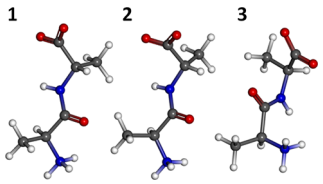

Figure 3. Conformations of alanine dipeptide. Three conformations of alanine dipeptide are shown, which result from a minimization in a Generalized Born solvent and which were afterward used in EC-RISM/QM (exact potential) and EC-RISM/AMOEBA calculations as well as for standard 3D RISM theory with AMBER ff99SB parameters.

where structures 1 and 2 were chosen as distinct minima belonging to the same conformational basin. With the fixed charge AMBER force field only a single 3D RISM calculation is necessary while the intramolecular energy apparently cannot change upon solvation in a fixed geometry in contrast to EC-RISM iterations. To judge the performance of the three methods employed, we computed pairwise differences of the standard Gibbs energy and its contributions, the solute energy ΔE and the excess-chemical potential μ^{ex} (see eq 7). The results are summarized in Table 3 for both the vacuum and converged EC-RISM data.

Obviously and somewhat unexpectedly, the fixed charge force field is capable of recovering results obtained with EC-RISM in combination with QM in terms of $\Delta G°$, whereas larger differences occur for the AMOEBA-based results. Taking a closer look at the energy contributions, we note that the relative excess chemical potential computed with EC-RISM/AMOEBA yields values close to $\Delta\mu^{ex}$ from EC-RISM/QM, whereas 3D RISM/AMBER reveals drastic differences of up to 10 kcal mol^{-1}. Thus, the large deviation of $\Delta G°$ for AMOEBA and the small one for AMBER with respect to QM originate from the solute energies. In accordance with the results presented for the *gauche*−*trans* equilibrium of 1,2-dichloroethane, the induced dipoles as the only polarizable term in the AMOEBA potential energy definition do not seem to sufficiently reproduce the change in the electronic structure of the solute. The AMBER results apparently benefit substantially from error compensation. To further investigate the outcome of the three methods, we illustrate the solvent site density distribution function in Figure 4. In agreement with the data in Table 3 for the excess chemical potential, the *g* functions obtained by AMBER exhibit evident differences to the EC-RISM-based methods.

Potential of Mean Force of a Water Dimer. The relevance of a polarizable force field for molecular associations can be best studied by computing the PMF. Since the AMOEBA water model has been calibrated by fitting to QM-derived dimer energies by correcting for the BSSE,[18] we compare EC-RISM/AMOEBA and EC-RISM/QM with and without accounting for the BSSE. Apparently, the results for both QM-based EC-RISM calculations differ by about 1 kcal mol^{-1} at most if the water molecules are in close proximity to

Table 3. Results for Alanine Dipeptide Conformations[a]

		$(1-2)_{vac}$	$(1-3)_{vac}$	$(2-3)_{vac}$	$(1-2)_{sol}$	$(1-3)_{sol}$	$(2-3)_{sol}$
$\Delta G°$							
	AMBER	−0.65	−2.82	−2.17	−0.65	−2.82	−2.17
	QM/pot	−1.19	−6.53	−5.34	−0.39	−3.48	−3.09
	AMOEBA	−4.28	−7.48	−3.20	−2.62	−2.20	0.42
ΔE							
	AMBER	−1.94	−9.13	−7.19	−1.94	−9.13	−7.19
	QM/pot	−3.06	−10.69	−7.63	−5.27	−20.26	−14.99
	AMOEBA	−5.83	−12.25	−6.42	−7.03	−16.83	−9.80
$\Delta\mu^{ex}$							
	AMBER	1.29	6.31	5.02	1.29	6.31	5.02
	QM/pot	1.87	4.16	2.29	4.87	16.77	11.90
	AMOEBA	1.55	4.77	3.22	4.41	14.63	10.22

[a]Relative values are shown for standard Gibbs energy $\Delta G°$, the solute energy ΔE and the excess chemical potential $\Delta\mu^{ex}$ both for the vacuum Hamiltonian and the converged solvated interaction energies (AMBER values are identical, independent of the environment). Data are listed in kcal mol^{-1} for each applied method, that is, 3D RISM with AMBER ff99SB parameters, EC-RISM/QM (exact potential) and EC-RISM/AMOEBA with AMOEBA-BIO-2009 parameters.

dx.doi.org/10.1021/ct400699q | J. Chem. Theory Comput. XXXX, XXX, XXX−XXX

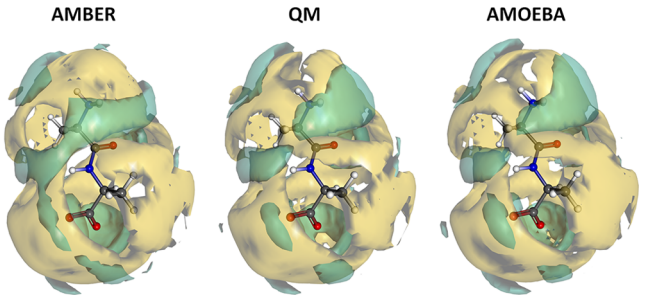

Figure 4. Pair distribution functions of alanine dipeptide structure 1 (see Figure 3). For both solvent sites O (yellow, isovalue 2.3) and H (cyan, isovalue 1.3) the solvent site density distribution is shown as derived from 3D RISM calculations with AMBER ff99SB parameters and EC-RISM calculations in combination with QM and AMOEBA.

each other. However, only BSSE-corrected data agree well with AMOEBA values at least close to the energetic minima; for the exact QM electrostatics the agreement with EC-RISM/AMOEBA in these regions is almost quantitative. As expected, the BSSE influence diminishes with larger distances. Obviously, the AMOEBA parametrization (including BSSE correction) captures the QM free energy surface quite well for stable states, but less accurately for barriers.

Again, we try to examine the reason for the observed deviation more closely by subdividing the free energy into its components. As can be seen in the lower panel of Figure 5, the discrepancy of the solvation contribution to the PMF in the barrier region is smaller than the total PMF difference, more pronounced for the exact electrostatics QM calculations. The agreement is much better in the minima regions, indicating that, here in contrast to previous benchmarks, the intramolecular energetics in solution are captured quite well by AMOEBA, which is possibly a consequence of the thorough parametrization of AMOEBA water, which focuses on adequate description of geometrical optima. However, the barrier deviations are again dominated by the deficiencies of the intramolecular terms which could be considered for future improvements.

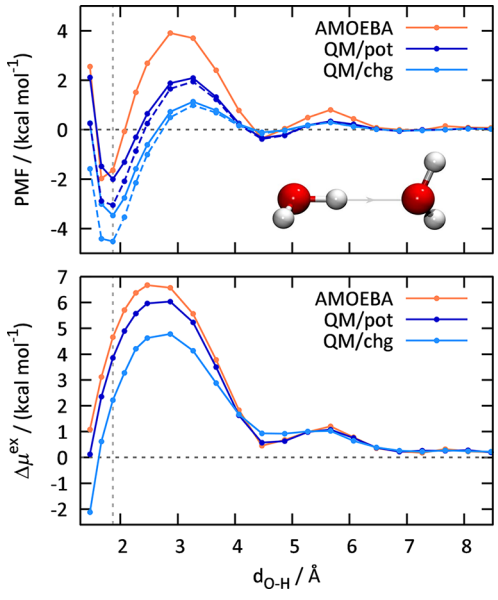

Figure 5. Potential of mean force for a water dimer. For a number of O−H distances of both water molecules (see inset of the upper panel) the PMF (upper panel) is calculated by normalizing the dimer standard Gibbs energy ΔG° to the corresponding monomer free energies. The QM energies (with point charges only, "QM/chg", and with the exact potential, "QM/pot") are shown with (solid lines) and without (dashed lines) BSSE correction. The lower panel shows the corresponding excess chemical potentials. The vertical dashed gray line denotes the minimum energy distance at 1.868 Å.

CONCLUSION

This study was intended as a proof of principle demonstration that polarizable force fields can be combined with granular implicit solvent models such as 3D RISM. We applied the presented methodology, EC-RISM/AMOEBA, to different test cases to evaluate its performance in comparison with EC-RISM/QM reference calculations. A consistent picture emerges for all applications in that we find close agreement between AMOEBA and QM for the excess chemical potential (i.e., solvation) contributions to the total free energy, which additionally contains the (polarizable) intramolecular energies. This is also reflected by the similarity of AMOEBA and QM solvent distribution functions.

In general, the intramolecular contributions deviate systematically stronger between QM and AMOEBA approaches although the agreement can be improved if the parametrization of AMOEBA torsion terms corresponds to the level chosen for pure QM calculations. Apparently, the induced dipole interaction potential as the only term that accounts for polarizability in AMOEBA is not sufficient for fully capturing the intramolecular polarization energy change upon solvation. Complementing our findings, Ren et al.[16] already pointed out the importance of the fact that polarizability effects are not yet coupled to valence potentials in a geometry-dependent manner which may be crucial for the design of novel polarizable force fields. This statement holds although we employed a repulsion−dispersion term that differs from the original AMOEBA formulation, as demonstrated by MD simulations.

These data indicate that the adequate treatment of intramolecular solute polarizability could be more important than explicit polarizability of the solvent, at least for the water case studied here, in agreement with Shi et al.[46] This statement, however, needs further investigation in the future since detailed studies of merging polarizable solute models with electronically unpolarizable solvents are rare, let alone in comparison with a fully polarizable setup. For instance, Shelley et al.[60] performed MD simulations of micelle structures for polarizable and unpolarizable ionic surfactant solutions in conjunction with a standard fixed-charge water model. They found little impact of polarizability on monomers but substantial effect on aggregate features. Cummings and co-workers[61] compared solubility data of polarizable and unpolarizable small solute models for standard water force fields and found that accounting for solute polarizability alone already leads to significant improvement. The challenge for future work in combining liquid state theory with molecular polarizability lies in adapting analytical theory for fully polarizable solvents (see for instance refs 62−65) to modern polarizable force field models.

As a perspective for future developments toward modeling changes of covalent bonding patterns such as for predicting for instance acidity or tautomer ratios with an accuracy comparable to EC-RISM/QM, the intramolecular terms are the relevant targets. EC-RISM/QM calculations could serve as a source for providing reference data in order to enhance polarizable force field parametrizations.

dx.doi.org/10.1021/ct400699q | J. Chem. Theory Comput. XXXX, XXX, XXX−XXX

AUTHOR INFORMATION

Corresponding Author

*E-mail: stefan.kast@tu-dortmund.de.

Notes

The authors declare no competing financial interest.

ACKNOWLEDGMENTS

We thank the German Federal Ministry of Education and Research (BMBF) and the German Research Foundation (DFG) for financial and the IT and Media Center (ITMC) of the TU Dortmund for computational support. Figures 2, 3, and 4 have been created using the MOLCAD software;[66] the inset in Figure 5 using VMD.[67] We are also grateful to Daniel Tomazic for his support with the setup and analysis of the MD simulation and to Jay Ponder and the reviewers for helpful comments on the manuscript.

ABBREVIATIONS

AMOEBA, atomic multipole optimized energetics for biomolecular applications; BSSE, basis set superposition error; EC, embedded cluster; GAFF, general Amber force field; (G)DMA, (Gaussian) distributed multipole analysis; HNC, hypernetted chain; MD, molecular dynamics; MP, Møller−Plesset; QM, quantum mechanics; PMF, potential of mean force; PSE, partial series expansion; RISM, reference interaction site model

REFERENCES

(1) Cieplak, P.; Dupradeau, F.-Y.; Duan, Y.; Wang, J. Polarization effects in molecular mechanical force fields. *J. Phys.: Condens. Matter* **2009**, *21*, 333102.

(2) Lopes, P. E. M.; Roux, B.; MacKerell, A. D., Jr. Molecular modeling and dynamics studies with explicit inclusion of electronic polarizability theory and applications. *Theor. Chem. Acc.* **2009**, *124*, 11−28.

(3) Sprik, M.; Klein, M. L. A polarizable model for water using distributed charge sites. *J. Chem. Phys.* **1988**, *89*, 7556−7560.

(4) Lamoureux, G.; Roux, B. Modeling induced polarization with classical Drude oscillators: Theory and molecular dynamics simulation algorithm. *J. Chem. Phys.* **2003**, *119*, 3025−3039.

(5) Lamoureux, G.; MacKerell, A. D., Jr.; Roux, B. A simple polarizable model of water based on classical Drude oscillators. *J. Chem. Phys.* **2003**, *119*, 5185−5197.

(6) Anisimov, V. M.; Lamoureux, G.; Vorobyov, I. V.; Huang, N.; Roux, B.; MacKerell, A. D., Jr. Determination of electrostatic parameters for a polarizable force field based on the classical Drude oscillator. *J. Chem. Theory Comput.* **2005**, *1*, 153−169.

(7) Rappe, A. K.; Goddard, W. A., III Charge equilibration for molecular simulation. *J. Phys. Chem.* **1991**, *95*, 3358−3363.

(8) Rick, S. W.; Stuart, S. J.; Berne, B. J. Dynamical fluctuating charge force fields: Application to liquid water. *J. Chem. Phys.* **1994**, *101*, 6141−6156.

(9) Banks, J. L.; Kaminski, G. A.; Zhou, R.; Mainz, D. T.; Berne, B. J.; Friesner, R. A. Parametrizing a polarizable force field from ab initio data: I. Fluctuating point charge model. *J. Chem. Phys.* **1999**, *110*, 741−754.

(10) Kaminski, G. A.; Stern, H. A.; Berne, B. J.; Friesner, R. A.; Cao, Y. X.; Murphy, R. B.; Zhou, R.; Halgren, T. A. Development of a polarizable force field for proteins via ab initio quantum chemistry: First generation model and gas phase tests. *J. Comput. Chem.* **2002**, *23*, 1515−1531.

(11) Caldwell, J.; Dang, L. X; Kollman, P. A. Implementation of nonadditive intermolecular potentials by use of molecular dynamics: Development of a water−water potential and water−ion cluster interactions. *J. Am. Chem. Soc.* **1990**, *112*, 9144−9147.

(12) Cieplak, P.; Kollman, P.; Lybrand, T. A new water potential including polarization: Application to gas-phase, liquid, and crystal properties of water. *J. Chem. Phys.* **1990**, *92*, 6755−6760.

(13) Dang, L. X.; Rice, J. E.; Caldwell, J.; Kollman, P. A. Ion solvation in polarizable water: Molecular dynamics simulation. *J. Am. Chem. Soc.* **1991**, *113*, 2481−2486.

(14) Bernardo, D. N.; Ding, Y.; Krogh-Jespersen, K.; Levy, R. M. An anisotropic polarizable water model: Incorporation of all-atom polarizabilities into molecular mechanics force fields. *J. Phys. Chem.* **1994**, *98*, 4180−4187.

(15) Ponder, J. W.; Wu, C.; Ren, P.; Pande, V. S.; Chodera, J. D.; Schnieders, M. J.; Haque, I.; Mobley, D. L.; Lambrecht, D. S.; DiStasio, R. A., Jr.; Head-Gordon, M.; Clark, G. N. I.; Johnson, M. E.; Head-Gordon, T. Current status of the AMOEBA polarizable force field. *J. Phys. Chem. B* **2010**, *114*, 2549−2564.

(16) Ren, P.; Wu, C.; Ponder, J. W. Polarizable atomic multipole-based molecular mechanics for organic molecules. *J. Chem. Theory Comput.* **2011**, *7*, 3143−3161.

(17) Ren, P.; Ponder, J. W. Consistent treatment of inter- and intramolecular polarization in molecular mechanics calculations. *J. Comput. Chem.* **2002**, *23*, 1497−1506.

(18) Ren, P.; Ponder, J. W. Polarizable atomic multipole water model for molecular mechanics simulation. *J. Phys. Chem. B* **2003**, *107*, 5933−5947.

(19) Ren, P.; Ponder, J. W. Temperature and pressure dependence of the AMOEBA water model. *J. Phys. Chem. B* **2004**, *108*, 13427−13437.

(20) Warshel, A.; Kato, M.; Pisliakov, A. V. Polarizable force fields: History, test cases, and prospects. *J. Chem. Theory Comput.* **2007**, *3*, 2034−2045.

(21) Grossfield, A.; Ren, P.; Ponder, J. W. Ion solvation thermodynamics from simulation with a polarizable force field. *J. Am. Chem. Soc.* **2003**, *125*, 15671−15682.

(22) Lamoureux, G.; Roux, B. Absolute hydration free energy scale for alkali and halide ions established from simulations with a polarizable force field. *J. Phys. Chem. B* **2006**, *110*, 3308−3322.

(23) Wu, J. C.; Piquemal, J.-P.; Chaudret, R.; Reinhardt, P.; Ren, P. Polarizable molecular dynamics simulation of Zn(II) in water using the AMOEBA force field. *J. Chem. Theory Comput.* **2010**, *6*, 2059−2070.

(24) Yu, H.; Whitfield, T. W.; Harder, E.; Lamoureux, G.; Vorobyov, I.; Anisimov, V. M.; MacKerell, A. D., Jr.; Roux, B. Simulating monovalent and divalent cations in aqueous solution using a Drude polarizable force field. *J. Chem. Theory Comput.* **2010**, *6*, 774−786.

(25) Kaminsky, J.; Jensen, F. Force field modeling of amino acid conformational energies. *J. Chem. Theory Comput.* **2007**, *3*, 1774−1788.

(26) Semrouni, D.; Ohanessian, G.; Clavaguera, C. Structural, energetic, and dynamical properties of sodiated oligoglycines: Relevance of a polarizable force field. *Phys. Chem. Chem. Phys.* **2010**, *12*, 3450−3462.

(27) Rasmussen, T. D.; Ren, P.; Ponder, J. W.; Jensen, F. Force field modeling of conformational energies: Importance of multipole moments and intramolecular polarization. *Int. J. Quantum Chem.* **2007**, *107*, 1390−1395.

(28) Schnieders, M. J.; Baker, N. A.; Ren, P.; Ponder, J. W. Polarizable atomic solutes in a Poisson−Boltzmann continuum. *J. Chem. Phys.* **2007**, *126*, 124114.

(29) Maple, J. R.; Cao, Y.; Damm, W.; Halgren, T. A.; Kaminski, G. A.; Zhang, L. Y.; Friesner, R. A. A polarizable force field and continuum solvation methodology for modeling of protein−ligand interactions. *J. Chem. Theory Comput.* **2005**, *1*, 694−715.

(30) Schnieders, M. J.; Ponder, J. W. Polarizable atomic multipole solutes in a generalized Kirkwood continuum. *J. Chem. Theory Comput.* **2007**, *3*, 2083−2097.

(31) Lipparini, F.; Barone, V. Polarizable force fields and polarizable continuum model: A fluctuating charges/PCM approach. 1. Theory and implementation. *J. Chem. Theory Comput.* **2011**, *7*, 3711−3724.

(32) Beglov, D.; Roux, B. An integral equation to describe solvation of polar molecules in liquid water. *J. Phys. Chem. B* **1997**, *101*, 7821−7826.

(33) Kovalenko, A.; Hirata, F. Three-dimensional density profiles of water in contact with a solute of arbitrary shape: A RISM approach. *Chem. Phys. Lett.* **1998**, *290*, 237−244.
(34) Kloss, T.; Heil, J.; Kast, S. M. Quantum chemistry in solution by combining 3D integral equation theory with a cluster embedding strategy. *J. Phys. Chem. B* **2008**, *112*, 4337−4343.
(35) Kast, S. M.; Heil, J.; Güssregen, S.; Schmidt, K. F. Prediction of tautomer ratios by embedded-cluster integral equation theory. *J. Comput.-Aided Mol. Des.* **2010**, *24*, 343−353.
(36) Ponder, J. TINKER Molecular Modeling Package. http://dasher.wustl.edu/tinker/ (accessed Sept. 12, 2013).
(37) Applequist, J.; Carl, J. R.; Fung, K.-K. An atom dipole interaction model for molecular polarizability. Application to polyatomic molecules and determination of atom polarizabilities. *J. Am. Chem. Soc.* **1972**, *94*, 2952−2960.
(38) Thole, B. T. Molecular polarizabilities calculated with a modified dipole interaction. *Chem. Phys.* **1981**, *59*, 341−350.
(39) van Duijnen, P. Th.; Swart, M. Molecular and atomic polarizabilities: Thole's model revisited. *J. Phys. Chem. A* **1998**, *102*, 2399−2407.
(40) Wu, J. C.; Chattree, G.; Ren, P. Automation of AMOEBA polarizable force field parameterization for small molecules. *Theor. Chem. Acc.* **2012**, *131*, 1138−1148.
(41) Frisch, M. J.; Trucks, G. W.; Schlegel, H. B.; Scuseria, G. E.; Robb, M. A.; Cheeseman, J. R.; Scalmani, G.; Barone, V.; Mennucci, B.; Petersson, G. A.; Nakatsuji, H.; Caricato, M.; Li, X.; Hratchian, H. P.; Izmaylov, A. F.; Bloino, J.; Zheng, G.; Sonnenberg, J. L.; Hada, M.; Ehara, M.; Toyota, K.; Fukuda, R.; Hasegawa, J.; Ishida, M.; Nakajima, T.; Honda, Y.; Kitao, O.; Nakai, H.; Vreven, T.; Montgomery, J. A., Jr.; Peralta, J. E.; Ogliaro, F.; Bearpark, M.; Heyd, J. J.; Brothers, E.; Kudin, K. N.; Staroverov, V. N.; Kobayashi, R.; Normand, J.; Raghavachari, K.; Rendell, A.; Burant, J. C.; Iyengar, S. S.; Tomasi, J.; Cossi, M.; Rega, N.; Millam, J. M.; Klene, M.; Knox, J. E.; Cross, J. B.; Bakken, V.; Adamo, C.; Jaramillo, J.; Gomperts, R.; Stratmann, R. E.; Yazyev, O.; Austin, A. J.; Cammi, R.; Pomelli, C.; Ochterski, J. W.; Martin, R. L.; Morokuma, K.; Zakrzewski, V. G.; Voth, G. A.; Salvador, P.; Dannenberg, J. J.; Dapprich, S.; Daniels, A. D.; Farkas, O.; Foresman, J. B.; Ortiz, J. V.; Cioslowski, J.; Fox, D. J. *Gaussian09*; Gaussian, Inc., Wallingford, CT, 2009.
(42) Stone, A. J. Distributed multipole analysis, or how to describe a molecular charge distribution. *Chem. Phys. Lett.* **1981**, *83*, 233−239.
(43) Stone, A. J.; Alderton, M. Distributed multipole analysis. Methods and applications. *Mol. Phys.* **1985**, *56*, 1047−1064.
(44) Stone, A. J. Distributed multipole analysis: Stability for large basis sets. *J. Chem. Theory Comput.* **2005**, *1*, 1128−1132.
(45) Bondi, A. van der Waals volumes and radii. *J. Phys. Chem.* **1964**, *68*, 441−451.
(46) Shi, Y.; Wu, C.; Ponder, J. W.; Ren, P. Multipole electrostatics in hydration free energy calculations. *J. Comput. Chem.* **2011**, *32*, 967−977.
(47) Kast, S. M.; Kloss, T. Closed-form expressions of the chemical potential for integral equation closures with certain bridge functions. *J. Chem. Phys.* **2008**, *129*, 236101.
(48) Morita, T.; Hiroike, K. Integral equation for pair distribution function. *Prog. Theor. Phys.* **1960**, *23*, 385−387.
(49) Kovalenko, A.; Hirata, F. Potentials of mean force of simple ions in ambient aqueous solution. I. Three-dimensional reference interaction site model approach. *J. Chem. Phys.* **2000**, *112*, 10391−10402.
(50) Joung, S.; Luchko, T.; Case, D. A. Simple electrolyte solutions: Comparison of DRISM and molecular dynamics results for alkali halide solutions. *J. Chem. Phys.* **2013**, *138*, 044103.
(51) Maw, S.; Sato, H.; Ten-no, S.; Hirata, F. Ab initio study of water: Self-consistent determination of electronic structure and liquid state properties. *Chem. Phys. Lett.* **1997**, *276*, 20−25.
(52) Frisch, M. J.; Trucks, G. W.; Schlegel, H. B.; Scuseria, G. E.; Rob, M. A.; Cheeseman, J. R.; Montgomery, J. A., Jr.; Vreven, T.; Kudin, K. N.; Burant, J. C.; Millam, J. M.; Iyengar, S. S.; Tomasi, J.; Barone, V.; Mennucci, B.; Cossi, M.; Scalmani, G.; Rega, N.; Petersson, G. A.; Nakatsuji, H.; Hada, M.; Ehara, M.; Toyota, K.; Fukuda, R.; Hasegawa, J.; Ishida, M.; Nakajima, T.; Honda, Y.; Kitao, O.; Nakai, H.; Klene, M.; Li, X.; Knox, J. E.; Hratchian, H. P.; Cross, J. B.; Bakken, V.; Adamo, C.; Jaramillo, J.; Gomperts, R.; Stratmann, R. E.; Yazyev, O.; Austin, A. J.; Cammi, R.; Pomelli, C.; Ochterski, J. W.; Ayala, P. Y.; Morokuma, K.; Voth, G. A.; Salvador, P.; Dannenberg, J. J.; Zakrzewski, V. G.; Dapprich, S.; Daniels, A. D.; Strain, M. C.; Farkas, O.; Malick, D. K.; Rabuck, A. D.; Raghavachari, K.; Foresman, J. B.; Ortiz, J. V.; Cui, Q.; Baboul, A. G.; Clifford, S.; Cioslowski, J.; Stefanov, B. B.; Liu, G.; Liashenko, A.; Piskorz, P.; Komaromi, I.; Martin, R. L.; Fox, D. J.; Keith, T.; Al-Laham, M. A.; Peng, C. Y.; Nanayakkara, A.; Challacombe, M.; Gill, P. M. W.; Johnson, B.; Chen, W.; Wong, M. W.; Gonzalez, C.; Pople, J. A. *Gaussian 03*; Gaussian, Inc., Wallingford, CT, 2003.
(53) Wang, J.; Wolf, R. M.; Caldwell, J. W.; Kollman, P. A.; Case, D. A. Development and testing of a general Amber force field. *J. Comput. Chem.* **2004**, *25*, 1157−1174.
(54) Cornell, W. D.; Cieplak, P.; Bayly, C. I.; Gould, I. R.; Merz, K. M., Jr.; Ferguson, D. M.; Spellmeyer, D. C.; Fox, T.; Caldwell, J. W.; Kollman, P. A. A second generation force field for the simulation of proteins, nucleic acids, and organic molecules. *J. Am. Chem. Soc.* **1995**, *117*, 5179−5197.
(55) Wang, J.; Cieplak, P.; Kollman, P. A. How well does a restrained electrostatic potential (RESP) model perform in calculating conformational energies of organic and biological molecules? *J. Comput. Chem.* **2000**, *21*, 1049−1074.
(56) Case, D. A.; Darden, T. A.; Cheatham III, T. E.; Simmerling, C. L.; Wang, J.; Duke, R. E.; Luo, R.; Walker, R. C.; Zhang, W.; Merz, K. M.; Roberts, B.; Hayik, S.; Roitberg, A.; Seabra, G.; Swails, J.; Goetz, A. W.; Kolossvary, I.; Wong, K. F.; Paesani, F.; Vanicek, J.; Wolf, R. M.; Liu, J.; Wu, X.; Brozell, S. R.; Steinbrecher, T.; Gohlke, H.; Cai, Q.; Ye, X.; Wang, J.; Hsieh, M.-J.; cui, G.; Roe, D. R.; Mathews, D. H.; Seetin, M. G.; Salomon-Ferrer, R.; Sagui, C.; Babin, V.; Luchko, T.; Gusarov, S.; Kovalenko, A.; Kollman, P. A. *AMBER12*; University of California: San Francisco, 2012.
(57) Tsui, V.; Case, D. A. Theory and applications of the generalized Born solvation model in macromolecular simulations. *Biopolymers* **2001**, *56*, 275−291.
(58) Tomasi, J.; Mennucci, B.; Cammi, R. Quantum mechanical continuum solvation models. *Chem. Rev.* **2005**, *105*, 2999−3093.
(59) Kato, M.; Abe, I.; Taniguchi, Y. Raman study of the *trans*−*gauche* conformational equilibrium of 1,2-dichloroethane in water: Experimental evidence for the hydrophobic effect. *J. Chem. Phys.* **1999**, *110*, 11982−11986.
(60) Shelley, J. C.; Sprik, M.; Klein, M. L. Molecular dynamics simulation of an aqueous sodium octanoate micelle using polarizable surfactant molecules. *Langmuir* **1993**, *9*, 916−926.
(61) Dyer, P. J.; Docherty, H.; Cummings, P. T. The importance of polarizability in the modeling of solubility: Quantifying the effect of solute polarizability on the solubility of small nonpolar solutes in popular models of water. *J. Chem. Phys.* **2008**, *129*, 024508.
(62) Wertheim, M. S. Theory of polar fluids. I. *Mol. Phys.* **1973**, *26*, 1425−1444.
(63) Pratt, L. R. Effective field of a dipole in nonpolar polarizable fluids. *Mol. Phys.* **1980**, *40*, 347−360.
(64) Høye, J. S.; Stell, G. Dielectric theory for polar molecules with fluctuating polarizability. *J. Chem. Phys.* **1980**, *73*, 461−468.
(65) Lado, F. Molecular theory of a charged particle in a polarizable nonpolar liquid. *J. Chem. Phys.* **1997**, *106*, 4707−4713.
(66) Molcad GmbH, Germany; http://www.molcad.de (accessed Sept. 12, 2013).
(67) Humphrey, W.; Dalke, A.; Schulten, K. VMD: Visual Molecular Dynamics. *J. Mol. Graphics* **1996**, *14*, 33−38.